Rock Mechanics and Rock Engineering (2022) 55:505–519
https://doi.org/10.1007/s00603-021-02693-8

ORIGINAL PAPER

Assessment of Tensorial and Scalar Damage Models for an Isotropic Thermally Cracked Rock Under Confining Pressure Using Experimental Data: Continuum Damage Mechanics Versus Effective Medium Theory

Louise Olsen-Kettle[1] · **Joel Sarout**[2]

Received: 22 April 2021 / Accepted: 17 October 2021 / Published online: 3 November 2021

Abstract
Many models of damage or cracking of isotropic solids consider a single damage/crack density variable. Based on both continuum damage mechanics (CDM) and effective medium theory (EMT), we model the impact of isotropic damage in the form of microcracks on the elastic properties of an isotropic solid. For each approach, we consider the complete tensorial description of the elastic moduli involving two damage/crack density variables D_1 and D_2, or α and β; and possible scalar approximations involving a single variable (with either $D_2 = 0$, or $\beta = 0$). We assess the accuracy of scalar approximations commonly employed for each approach against laboratory measurements of ultrasonic wave velocities and density obtained on a dry and isotropic specimen of thermally cracked Carrara Marble (CM) subjected to an increasing confining pressure up to 50 MPa. Overall, this laboratory dataset and the CDM and EMT modelling and inversion results reported here suggest that: (i) irreversible thermal cracking and microcrack opening occur after heating and sudden cooling of the CM specimen, whereas reversible and progressive microcracks' closure occurs with increasing confining pressure; (ii) tensorial damage/cracking models involving either two damage variables (CDM) or two crack density variables (EMT) fit equally well and virtually perfectly the laboratory data for any confining pressure tested; (iii) single scalar approximation models commonly used in CDM or the EMT models give comparable results to their complete tensorial counterparts, which is particularly true for the CDM approach; (iv) single scalar approximations derived from the CDM approach, and assuming a constant Poisson's ratio of the cracked rock, reproduces all the elastic moduli more accurately than the corresponding scalar approximation derived from the EMT approach, where a constant ratio of Young's modulus to Poisson's ratio is assumed instead; and (v) it is more reliable to use a tensorial rather than a scalar description of the effect of reversible microcrack closure with pressure on all elastic parameters, including Poisson's ratio. If the impact of reversible microcrack closure is accounted for, then a single scalar description of irreversible thermal damage with the CDM approach is remarkably accurate.

Keywords Continuum damage mechanics · Effective medium theory · Damage tensor · Crack density tensor · Microcrack closure · Thermal cracking · Ultrasonic wave velocities · Confining pressure

1 Introduction

Laboratory ultrasonic monitoring techniques provide a fast and non-destructive means for estimating the elastic properties of a damaged/cracked solid. Ultrasonic probing has been widely employed in many fields (e.g., material science, geoscience). Many researchers have successfully used them to identify the parameters of phenomenological models of anisotropic damage in composite materials (e.g., Audoin and Baste 1994; Hufenbach et al. 2006; Castellano et al. 2017; Olsen-Kettle 2018a, c, b). However, purely phenomenological models alone do not lend themselves well for a quantitative distinction between reversible microcrack opening/closure and irreversible damage processes. We extend these efforts to overcome this limitation and develop an approach to separate these effects using ultrasonic monitoring of ultrasonic wave velocities under varying confining pressure rather than at room conditions only.

✉ Louise Olsen-Kettle
lolsenkettle@swin.edu.au

[1] School of Science, Computing and Engineering Technologies, Mathematics Department, Swinburne University of Technology, Hawthorn, VIC, Australia

[2] CSIRO Energy, Perth, WA, Australia

Natural rocks contain pre-existing flaws and defects at a variety of length scales, from microscopic cracks to macroscopic fissures, joints and even continental faults. A number of studies have explored the effect of microcrack closure, healing and sealing on macroscopic rock properties, showing time-dependent restrengthening and permeability reduction under hydrothermal conditions (Brantut 2015). Seismic wave speed recovery due to crack or microcrack closure has been investigated by many authors in fault zones (Brantut 2015; Kaproth and Marone 2014). Earthquake faults rupture and restrengthen repeatedly during the seismic cycle. Faults restrengthen via a set of processes known collectively as fault healing, which are well documented in the laboratory but less well understood in tectonic fault zones (Kaproth and Marone 2014). On the other hand, self-healing technologies and materials are emerging as a promising approach to extend the service life of infrastructures and engineered materials. Ultrasonic probing methods are often employed to test the self-healing capacity of engineered materials (Ahn et al. 2017; Ouarabi et al. 2017). The effects of closure of pre-existing cracks in the first stage of initial and rapid strain hardening under increasing confining pressure are often ignored in models of damage for brittle engineered materials such as composites.

Accounting for the apparent stiffness recovery and increase in ultrasonic wave speeds due to microcrack closure is pivotal in ultrasonic investigations of damage and healing in composites and self-healing materials. In this context, microcracks closure and opening in response to changing isotropic stress (confining pressure) is a reversible process, whereas thermally induced cracking and chemical healing are irreversible processes. An understanding and quantitative discrimination between these processes would help in developing more accurate models of both healing and damage.

In this work we use existing damage/crack models to discriminate the effect on the elastic moduli of reversible strain hardening associated with increase in confining pressure and microcrack closure, from the irreversible thermally induced cracking of an isotropic specimen of Carrara Marble (CM) (Sarout et al. 2017). We deem microcrack closure and opening due to the respective application and removal of a confining pressure to be a reversible effect on the measured ultrasonic wave speeds. We consider the residual reduction in the measured ultrasonic wave speeds (when compared with the intact specimen which has not undergone thermal cracking) after the application of a confining pressure to be the remaining irreversible effect on the measured ultrasonic wave speeds which remains constant (irreversible) with or without a confining pressure applied. The confining pressure was applied to allow us to isolate the effect of the irreversible thermally induced cracking from the effect of reversible microcrack opening and closure on the measurement of the ultrasonic wave speeds.

To measure the damage due to thermal cracking we record the evolution of ultrasonic wave speeds with confining pressure in a thermally cracked specimen of Carrara marble. However, the ultrasonic measurements will integrate both the reversible effects of microcrack opening, the impact of which can be partially cancelled by application of a compressive stress, as well as the irreversible cracking, the impact of which is not totally cancelled by application of an arbitrarily high confining pressure. To discriminate between reversible and irreversible damage we subject the specimen to a stepwise increase in confining pressure to cause the microcracks to progressively close, while monitoring the evolution of ultrasonic wave speeds. As the confining pressure increases, we observe that the elastic moduli approach asymptotic values. The difference between these asymptotic values and the values of elastic parameters of the intact rock constitutes the irreversible part of the damage induced by thermal cracking.

Past studies have focused on the effect of microcracking in brittle solids on Poisson's ratio and Young's modulus (Zimmerman 1985; Bristow 1960; Walsh 1965b) or on the ratio of these two parameters as in Walsh (1965a) or Case (1984). Case (1984) compares several microcracking-elasticity theories and recasts these theories in terms of macroscopic parameters, Young's modulus and Poisson's ratio. We extend this analysis further by considering the effect of both thermal cracking of a marble specimen on its elastic moduli, as well as the effect of reversible microcrack closure by an increase in the confining pressure. We compare the accuracy of two well-known approaches for modelling damage/cracking behaviour: using continuum damage mechanics (CDM) and micro-mechanics based effective medium theory (EMT). When a fourth order tensor is used for both the damage variable D in CDM (Eq. 4) and additional compliance tensor ΔS in the EMT (Eq. 12) we show that the two approaches are completely described using measurements of ultrasonic longitudinal and shear wave velocities and densities at multiple confining pressures. These data yield estimates of the two independent dynamic elastic moduli of the damaged/cracked and isotropic rock at any given confining pressure. For each model, the single-scalar approximation essentially reduces the number of variables required to describe damage. The motivation for assessing the accuracy of the single-scalar approximations of the EMT and CDM models is that these approximations are more widely used for industrial applications because of their relative simplicity compared to more advanced and research-oriented tensorial models. To the authors' knowledge this study is the first comparing quantitatively the performance of the EMT and CDM models, and their single-scalar approximation, against laboratory measurements under variable pressure.

Quantifying the evolution of the damage or crack density variables with confining pressure in a representative rock

sample from ultrasonic wave speed and density data allows for the prediction of the evolution of the elastic properties of the rock with pressure or depth using the CDM and EMT models. The output of the tensorial (complete) version of these models match equally well the laboratory data, i.e., negligible discrepancies (see Fig. 3). However, the single-scalar approximations of the CDM and EMT models can introduce discrepancies that are evaluated and compared to assess their performance (see Fig. 3). For this evaluation we use the data derived from a thermally cracked sample of Carrara marble. Comparing the two approaches and their underlying assumptions, as well as the performance of their single-scalar approximation are the key aims of this manuscript.

The two approaches only consider diffuse damage due to thermal cracking of a Carrara marble specimen (no crack clustering, nor high crack density). The wavelength of the ultrasonic wave velocities measured on this rock (few mm) are significantly larger than the size of the micro-cracks observed in it (few microns). We therefore assume that both CDM and EMT approaches are applicable, as long as the crack density is low, and no crack clustering occurs.

We compare the results of two well-established approaches for modelling mechanical damage and cracking in solids: (i) thermodynamics-based continuum damage mechanics (CDM); and (ii) and micromechanics-based effective medium Theory (EMT). The thermodynamic theory of CDM considers the decrease in the elastic stiffness tensor with increasing crack damage (see Eq. (1)). The CDM approach introduces a thermodynamic damage variable (scalar or tensor) to model the overall (effective) effect of microcracking and damage at the scale of a representative volume element, rather than the contribution of each individual crack (Murakami 2012). This approach is based on energy conservation principles and is detailed in Sect. 2.

In contrast, the EMT requires the definition of an explicit damage model, i.e., micro-cracks geometry and spatial/orientation distribution. We assume here randomly located and oriented non-interacting and non-intersecting cracks, and a simple crack geometry (penny-shaped) in the thermally cracked CM specimen. The non-interaction EMT has been shown to be valid for cracked solids up to relatively high crack density values, i.e., even when the cracks become closely spaced and intersect (Kachanov 1993; Sayers and Kachanov 1995; Grechka and Kachanov 2006). In this approximation, each crack is assumed to be isolated and the additional elastic compliance of the cracked rock compared to the intact one (ΔS_{ijkl}) is simply the sum of the compliance contribution of each crack taken separately (see Eq. (9)). Thus, the EMT allows us to relate the change in the effective compliance tensor of the cracked rock (ΔS_{ijkl}) to the change in crack density (Walsh 1965b; Sarout et al. 2017), where the crack density characterizes the state of damage of the solid, and is a combination of the cubed radius of the cracks and their number per unit volume. This approach is detailed in Sect. 3.

The fourth order tensor D defined in Sect. 2 (Eq. (1)) represents a decrease in the elastic stiffness tensor with damage using CDM. Similarly the extra compliance tensor, ΔS, defined in Sect. 3 (Eq. (9)) represents an increase in the compliance tensor with damage. Obviously these will be related to each other and can be equivalent representations of the damage if a fourth order tensor is used for both. However in many studies further approximations are made to simplify the application of these tensorial models. We consider these commonly-adopted single-scalar approximations, and evaluate their performance. To this end, we assess the relative accuracy and predictive power of each model in terms of predicted elastic parameters (bulk, shear and Young's moduli, Poisson's ratio and P-wave modulus), against laboratory measurements of ultrasonic P- and S-wave velocities and density obtained at room temperature on a dry specimen of thermally cracked CM specimen subjected to an increasing confining pressure up to 50 MPa (Sarout et al. 2017).

Sarout et al. (2017) showed that the CM specimen retained its isotropy at room pressure after thermal cracking and could be conveniently modelled as an isotropic elastic solid embedding randomly-oriented and located microcracks (see Fig. 1). When subjected to an increasing confining pressure (isotropic stress), the cracked rock specimen is expected to retain its isotropy (Curie's principle, Curie (1894), Rasolofosaon (1998)). In addition, the wavelength of the ultrasonic waves propagating in the CM specimen (about 5 mm) is significantly larger than the characteristic size of the grains and inter-granular microcracks (about 150micron). The continuum assumption underlying both modelling approaches is therefore satisfied, i.e., the size of the Representative Volume Element (RVE) corresponding to the probing ultrasonic wavelength is much larger than the characteristic size of the heterogeneities/discontinuities (grains, microcracks) embedded in this RVE. It is also worth noting that in the CDM approach the reduction of the stiffness tensor components with damage is modelled, whereas the EMT approach models the increase in the compliance tensor components with damage. Furthermore, in view of the timescale of the experiment at room temperature (few hours), and the absence of pore fluid saturating the microcrack network, it is assumed that no significant time-dependent effects are at play during the experiment (e.g., chemical dissolution/precipitation, creep).

In Sect. 2 the fourth order tensor D_{ijkl} representing damage in the thermodynamics-based CDM approach is derived using the formulation reported by Cauvin and Testa (1999a). Assuming that Poisson's ratio remains constant and independent of damage, two approximate models are derived in terms of a single scalar damage variable D^{SC}

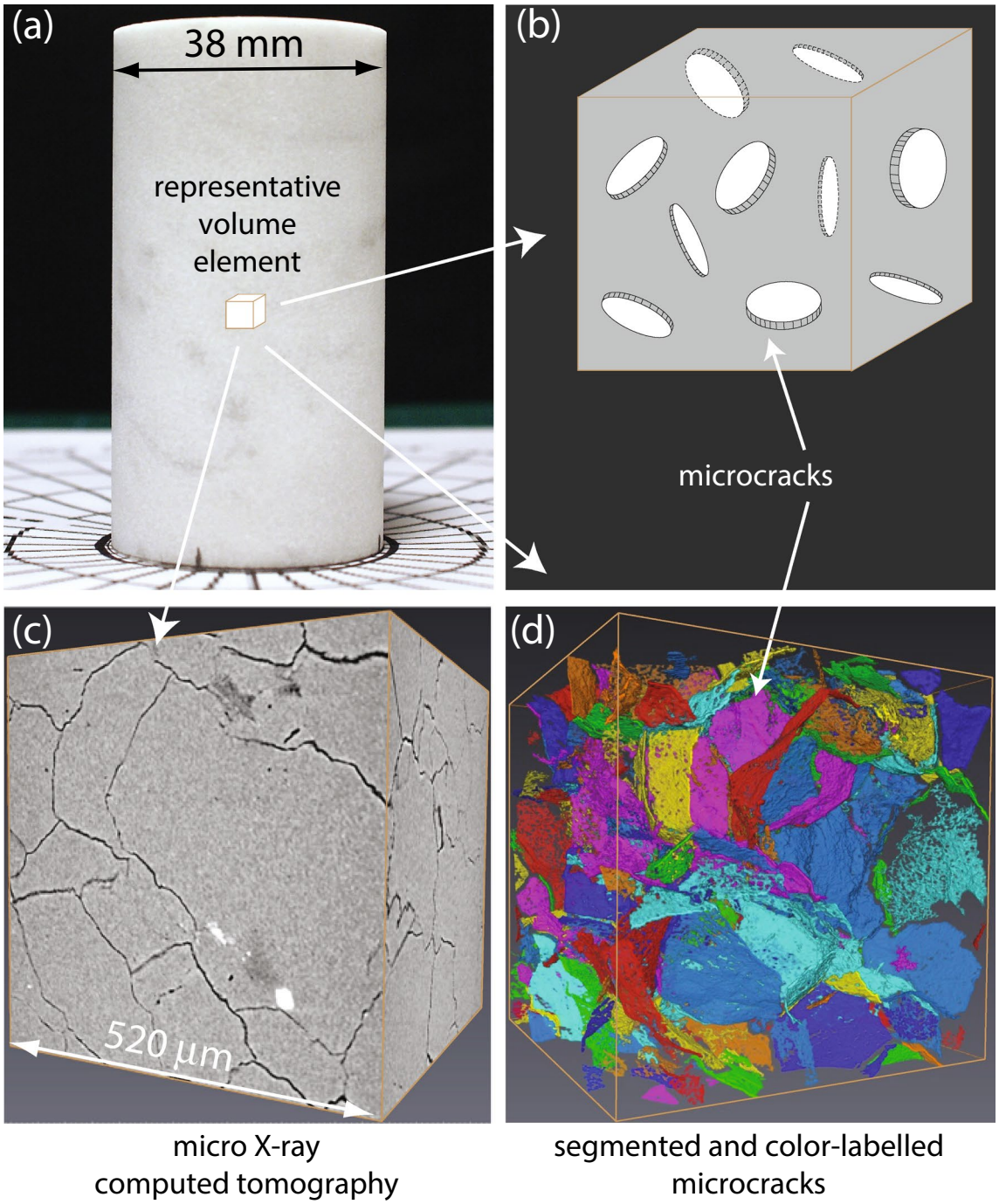

Fig. 1 Carrara Marble (CM) specimen: **a** picture of the specimen; **b** microstructural model of the isotropic CM specimen; **c** micro-X-ray computed tomography image of a half-millimetre cube of CM; **d** segmented X-ray image illustrating the presence of inter-granular microcracks

or D_E^{SC}. In Sect. 3 we model the presence of microcracks using a micromechanics-based EMT approach formulated by Sayers and Kachanov (1995). Assuming that the ratio of the Young's modulus to Poisson's ratio remains constant and independent of damage, two other approximate models are derived in terms of a single scalar crack density variable α^{SC} or α_E^{SC}. In Sect. 4 we analyze the ultrasonic laboratory data reported by Sarout et al. (2017) and invert for the damage or crack density parameters for the complete tensorial models and their scalar approximations. A discussion of the results and conclusions follow.

2 Continuum Damage Mechanics: Tensorial Description of Damage and Scalar Approximations

2.1 General Anisotropic Damage Tensor

We consider a general tensorial description of the effects of damage and microcrack opening and closure in an isotropic, thermally cracked Carrara Marble (CM) specimen subjected to increasing confining pressure (isotropic stress). To this end, we employ a similar approach to Olsen-Kettle (2018a, 2018c, 2018b) or Cauvin and Testa (1999a, 1999b) based on the principle of strain equivalence, and describe damage with an internal damage tensor D. The constitutive equations and the evolution of internal damage derive from thermodynamics principles of energy conservation involving stress and strain as internal state variables, and by postulating the mechanical equivalence between the damaged material and a fictitious undamaged material with the same properties (e.g., Murakami 2012).

The principle of strain equivalence considers two configurations: (i) the damaged configuration $\sigma = \tilde{C} : \epsilon$, where σ is the actual stress tensor, $\tilde{C}$ is the stiffness tensor of the damaged material, and ϵ is the actual strain tensor; and (ii) the fictitious undamaged configuration $\tilde{\sigma} = C : \epsilon$, where C is the original stiffness tensor of the undamaged material, $\tilde{\sigma}$ is the effective stress tensor applied to this equivalent undamaged material to generate the same elastic strain tensor ϵ. Using this concept, Cauvin and Testa (1999a) showed that the most general description of damage reduces to a fourth-order tensor D, i.e.,

$$\begin{aligned} &\tilde{C}_{ijkl} = (I_{ijrs} - D_{ijrs})C_{rskl}, \\ &\text{and } I_{ijrs} = \frac{1}{2}(\delta_{ir}\delta_{js} + \delta_{is}\delta_{jr}), \end{aligned} \tag{1}$$

where D_{ijkl} is the internal damage tensor and δ_{ij} is the Kronecker delta function. Because the stiffness tensors C and $\tilde{C}$ are supersymmetric D must possess minor symmetries: $D_{ijkl} = D_{jikl} = D_{ijlk}$. In addition, for the stiffness tensors to meet the constraint of supersymmetry, the internal damage tensor must also satisfy

$$D_{ijrs}C_{rskl} - D_{klrs}C_{rsij} = 0. \tag{2}$$

Note that the above equations hold for an arbitrary material symmetry.

2.2 Isotropic Damage Tensor

The above tensorial description of general anisotropic damage can be readily simplified to the case of isotropy for application to the ultrasonic and density data from the isotropic thermally cracked CM specimen. The stiffness tensor of the intact and isotropic CM specimen in Voigt notation reads (Cauvin and Testa 1999a, b; Voigt 1910; Helbig 1994)

$$C = \begin{pmatrix} \lambda+2G & \lambda & \lambda & 0 & 0 & 0 \\ \lambda & \lambda+2G & \lambda & 0 & 0 & 0 \\ \lambda & \lambda & \lambda+2G & 0 & 0 & 0 \\ 0 & 0 & 0 & G & 0 & 0 \\ 0 & 0 & 0 & 0 & G & 0 \\ 0 & 0 & 0 & 0 & 0 & G \end{pmatrix},$$

where λ and G stand for Lamè's parameters of the intact/undamaged specimen. The stiffness tensor of the thermally cracked and isotropic CM specimen can be written in a similar way, involving the corresponding Lamè's parameters of the specimen in a damaged state $\tilde{\lambda}$ and $\tilde{G}$, i.e.,

$$\tilde{C} = \begin{pmatrix} \tilde{\lambda}+2\tilde{G} & \tilde{\lambda} & \tilde{\lambda} & 0 & 0 & 0 \\ \tilde{\lambda} & \tilde{\lambda}+2\tilde{G} & \tilde{\lambda} & 0 & 0 & 0 \\ \tilde{\lambda} & \tilde{\lambda} & \tilde{\lambda}+2\tilde{G} & 0 & 0 & 0 \\ 0 & 0 & 0 & \tilde{G} & 0 & 0 \\ 0 & 0 & 0 & 0 & \tilde{G} & 0 \\ 0 & 0 & 0 & 0 & 0 & \tilde{G} \end{pmatrix}.$$

In practice, the same fourth-order internal damage tensor D is used to: (i) quantify the irreversible damage of the CM specimen due to thermal cracking; and (ii) quantify the reversible crack closure/opening with changing confining pressure. Discriminating between the two processes requires laboratory data to be collected at multiple confining pressures as reported by Sarout et al. (2017). In Voigt notation D can be written as (Cauvin and Testa 1999b)

$$D = \begin{pmatrix} D_1 & D_2 & D_2 & 0 & 0 & 0 \\ D_2 & D_1 & D_2 & 0 & 0 & 0 \\ D_2 & D_2 & D_1 & 0 & 0 & 0 \\ 0 & 0 & 0 & D_1-D_2 & 0 & 0 \\ 0 & 0 & 0 & 0 & D_1-D_2 & 0 \\ 0 & 0 & 0 & 0 & 0 & D_1-D_2 \end{pmatrix},$$

$$\text{or } D = \begin{pmatrix} D_{1111} & D_{1122} & D_{1133} & 0 & 0 & 0 \\ D_{2211} & D_{2222} & D_{2233} & 0 & 0 & 0 \\ D_{3311} & D_{3322} & D_{3333} & 0 & 0 & 0 \\ 0 & 0 & 0 & D_{2323} & 0 & 0 \\ 0 & 0 & 0 & 0 & D_{1313} & 0 \\ 0 & 0 & 0 & 0 & 0 & D_{1212} \end{pmatrix}.$$

Using Eq. (1) and the definition of the stiffness and internal damage tensors above, we can relate the two independent damage variables D_1 and D_2 to the laboratory-determined elastic moduli of the CM specimen in the damaged and undamaged states (Cauvin and Testa 1999b). A convenient relation can be obtained for the couple of independent elastic parameter K (bulk modulus) and G, i.e.,

$$\tilde{K} = (1 - D_1 - 2D_2)K,$$
$$\tilde{G} = (1 - D_1 + D_2)G. \tag{3}$$

The reciprocal equations can be written as

$$D_1 = 1 - \frac{1}{3}\left(2\frac{\tilde{G}}{G} + \frac{\tilde{K}}{K}\right),$$
$$D_2 = \frac{1}{3}\left(\frac{\tilde{G}}{G} - \frac{\tilde{K}}{K}\right). \tag{4}$$

As a result, isotropic damage can be fully described by two Eqs. (either (3) or (4)), using two independent damage variables D_1 and D_2.

2.3 Scalar Approximations of Isotropic Damage Tensor

In many continuum damage models (e.g., Lemaitre 1996; Zhu and Tang 2004; Murakami 2012; Li et al. 2012; Mondal et al. 2019, 2020) a single scalar damage variable is used to describe isotropic damage. In general these models assume that Poisson's ratio of the material is independent of damage, i.e.,

$$\nu = \tilde{\nu},$$

which is equivalent to assuming that the second damage variable D_2 is zero (Cauvin and Testa 1999b), and a single damage variable $D_1 = D^{SC}$ is sufficient in this case. A direct consequence of this assumption is that all elastic moduli are affected by damage in the same proportion (but not Poisson's ratio which is assumed constant in this approximation). In other words, in this approximation all elastic moduli exhibit strictly the same dependence to D^{SC}, e.g.,

$$\tilde{K} \approx (1 - D^{SC})K,$$
$$\tilde{G} \approx (1 - D^{SC})G. \tag{5}$$

Note that because only two independent elastic parameters are necessary and sufficient to fully describe the elastic response of an isotropic rock (intact or damaged), the other elastic parameters such as Young's modulus or Poisson's ratio can be readily calculated form K and G provided in Eq. (5) using classical elasticity relationships.

Let us investigate the validity of this assumption of constant Poisson's ratio, or dependence of elastic moduli on a single internal damage variable $D^{SC} = D_1$, using existing laboratory ultrasonic and density data for the CM specimen. Because two independent ultrasonic wave velocities are measured in the laboratory (P- and S-wave), we can estimate the two independent elastic moduli of the isotropic rock in the intact state K and G, and in a damaged state $\tilde{K}$ and $\tilde{G}$. One can readily compute any other elastic parameter from these two.

Using the known values of K_{exp} and G_{exp} for the defectless fused aggregate of pure calcite grains, and $\tilde{K}_{\text{exp}}$ and $\tilde{G}_{\text{exp}}$ calculated from the ultrasonic and density data reported by Sarout et al. (2017) on the CM specimen under increasing confining pressure, and using Eq. (5) allows us to estimate D^{SC} independently from the bulk modulus data on one hand, and from the shear modulus data on the other, i.e.,

$$D_K^{SC} \approx 1 - \frac{\tilde{K}_{\text{exp}}}{K_{\text{exp}}},$$
$$D_G^{SC} \approx 1 - \frac{\tilde{G}_{\text{exp}}}{G_{\text{exp}}}. \tag{6}$$

Let us consider two approaches for estimating the scalar damage variable from laboratory data. The first method makes use of both P- and S-wave velocity input data to compute the independent bulk and shear of the isotropic rock in the intact and damaged states. Equation (6) is then used to calculate the corresponding D_K^{SC} and D_G^{SC}. Finally, the experimentally-determined scalar damage variable D^{SC} is taken as the average of D_K^{SC} and D_G^{SC}, i.e.,

$$D^{SC} \approx \frac{1}{2}\left(D_K^{SC} + D_G^{SC}\right),$$
$$\approx 1 - \frac{1}{2}\left(\frac{\tilde{K}_{\text{exp}}}{K_{\text{exp}}} + \frac{\tilde{G}_{\text{exp}}}{G_{\text{exp}}}\right). \tag{7}$$

Often in the literature, triaxial stress-strain data are used to determine Young's modulus and estimate damage (e.g., Mondal et al. 2019, 2020). In order to better compare our results with previous data and models we also consider a second approximate damage variable D_E^{SC} directly based on experimentally-determined Young's modulus in the intact and damaged states, i.e.,

$$D_E^{SC} \approx 1 - \frac{\tilde{E}_{\text{exp}}}{E_{\text{exp}}},$$
$$\approx 1 - \frac{\frac{1}{K_{\text{exp}}} + \frac{3}{G_{\text{exp}}}}{\frac{1}{\tilde{K}_{\text{exp}}} + \frac{3}{\tilde{G}_{\text{exp}}}}. \tag{8}$$

Note that K_{exp} and G_{exp} are the elastic moduli of the intact (undamaged) rock material; and $\tilde{K}_{\text{exp}}$ and $\tilde{G}_{\text{exp}}$ are the elastic moduli of the damaged rock material estimated from laboratory ultrasonic and density data under increasing confining pressure by Sarout et al. (2017). Because Carrara marble is made of 98% calcite, the intact material properties are derived from the properties of a fused aggregate of randomly-oriented calcite grains with no porosity, no microcracks or other defects ($K_{\text{calcite}} = 80\,\text{GPa}$, and $G_{\text{calcite}} = 30\,\text{GPa}$).

3 Effective Medium Theory: Tensorial Description of Microcracks and Scalar Approximations

3.1 General Anisotropic Crack Density Tensors

The EMT approach considers first the effect on elastic moduli of a single inclusion embedded in a homogeneous and defect-free elastic solid. An upscaling scheme is then used to account for multiple such inclusions embedded in a Representative Volume Element (RVE) of the damaged CM specimen. The quantification of the effect of a single inclusion is rooted in Eshelby's equivalent/eigenstrain concept for elliptical inclusions (Eshelby 1957), which can be extended asymptotically to penny-shaped cracks. A classical upscaling scheme used for cracks consists in considering a simple superposition of the effect of multiple cracks with no stress interactions between them (Kachanov 1980, 1993; Sarout et al. 2007).

Embedding cracks into an elastic solid and using the non-interaction upscaling scheme, Sayers and Kachanov (1995) show that the average macroscopic strain (ϵ_{ij}) in an elastic volume element containing randomly located and non-interacting penny-shaped microcracks can be described by an increase in the elastic compliance of the microcracked material compared to the intact material, i.e.,

$$\begin{aligned} \epsilon_{ij} &= \left(S_{ijkl} + \Delta S_{ijkl}\right)\sigma_{kl} = \tilde{S}_{ijkl}\,\sigma_{kl}, \\ \text{and } \Delta S_{ijkl} &= \frac{1}{4}\left(\delta_{ik}\alpha_{jl} + \delta_{il}\alpha_{jk} + \delta_{jk}\alpha_{il} + \delta_{jl}\alpha_{ik}\right) + \beta_{ijkl}, \end{aligned} \tag{9}$$

where S_{ijkl} and $\tilde{S}_{ijkl}$ stand for the fourth-order elastic compliance tensor of the original intact material, and of the microcracked material, respectively. ΔS_{ijkl} is the additional compliance due to the presence of the microcracks, and can be conveniently decomposed into a second-order crack density tensor α_{ij}, and a fourth-order crack density tensor β_{ijkl}. The non-zero components of the crack density tensors and their relationship with the effective elastic parameters of the microcracked rock are given in detail by Sayers and Kachanov (1995) for various crack orientation distributions.

3.2 Isotropic Crack Density Tensors

For randomly located and oriented microcracks embedded in a homogeneous and isotropic elastic solid, Eq. (9) reduces to

$$\begin{aligned} \alpha &= \alpha_{11} = \alpha_{22} = \alpha_{33}, \\ \beta &= \beta_{1111} = \beta_{2222} = \beta_{3333}, \\ \frac{\beta}{3} &= \beta_{1122} = \beta_{2233} = \beta_{1133}\,(= \beta_{1212} = \beta_{2323} = \beta_{1313}). \end{aligned}$$

In Voigt notation, the compliance tensor $\tilde{S}$ of the isotropic damaged material reads

$$\begin{aligned} \tilde{S} &= \frac{1}{\tilde{E}}\begin{pmatrix} 1 & -\tilde{\nu} & -\tilde{\nu} & 0 & 0 & 0 \\ -\tilde{\nu} & 1 & -\tilde{\nu} & 0 & 0 & 0 \\ -\tilde{\nu} & -\tilde{\nu} & 1 & 0 & 0 & 0 \\ 0 & 0 & 0 & 2(1+\tilde{\nu}) & 0 & 0 \\ 0 & 0 & 0 & 0 & 2(1+\tilde{\nu}) & 0 \\ 0 & 0 & 0 & 0 & 0 & 2(1+\tilde{\nu}) \end{pmatrix} \\ &= \frac{1}{E}\begin{pmatrix} 1 & -\nu & -\nu & 0 & 0 & 0 \\ -\nu & 1 & -\nu & 0 & 0 & 0 \\ -\nu & -\nu & 1 & 0 & 0 & 0 \\ 0 & 0 & 0 & 2(1+\nu) & 0 & 0 \\ 0 & 0 & 0 & 0 & 2(1+\nu) & 0 \\ 0 & 0 & 0 & 0 & 0 & 2(1+\nu) \end{pmatrix} \\ &+ \begin{pmatrix} \alpha+\beta & \frac{\beta}{3} & \frac{\beta}{3} & 0 & 0 & 0 \\ \frac{\beta}{3} & \alpha+\beta & \frac{\beta}{3} & 0 & 0 & 0 \\ \frac{\beta}{3} & \frac{\beta}{3} & \alpha+\beta & 0 & 0 & 0 \\ 0 & 0 & 0 & 2\alpha+\frac{4\beta}{3} & 0 & 0 \\ 0 & 0 & 0 & 0 & 2\alpha+\frac{4\beta}{3} & 0 \\ 0 & 0 & 0 & 0 & 0 & 2\alpha+\frac{4\beta}{3} \end{pmatrix}, \end{aligned} \tag{10}$$

where ν and $\tilde{\nu}$ are the Poisson's ratio of the intact and cracked material respectively, and E and $\tilde{E}$ are the Young's modulus of the intact and cracked material respectively. Effective elastic parameters, $\tilde{E}, \tilde{\nu}$, can be related to the crack density variables and initial elastic moduli E, ν using Eq. (10). The additional relations of isotropic elasticity give the corresponding effective bulk modulus ($\tilde{K} = \tilde{E}/3(1-2\tilde{\nu})$) and effective shear modulus ($\tilde{G} = \tilde{E}/2(1+\tilde{\nu})$), i.e.,

$$\begin{aligned} \tilde{K} &= \frac{K}{1+K(3\alpha+5\beta)}, \\ \tilde{G} &= \frac{3G}{3+G(6\alpha+4\beta)}. \end{aligned} \tag{11}$$

The reciprocal set of equations equivalent to Eq. (4) in the CDM approach and relating the elastic parameters K and G to the crack density variables α and β in the EMT approach reads

$$\begin{aligned} \alpha &= \frac{5}{6}\left(\frac{1}{\tilde{G}} - \frac{1}{G}\right) - \frac{2}{9}\left(\frac{1}{\tilde{K}} - \frac{1}{K}\right), \\ \beta &= \frac{1}{3}\left(\frac{1}{\tilde{K}} - \frac{1}{K}\right) - \frac{1}{2}\left(\frac{1}{\tilde{G}} - \frac{1}{G}\right). \end{aligned} \tag{12}$$

3.3 Scalar Approximation of Isotropic Crack Density Tensors

The most common assumption made in micromechanical models for dry cracked rocks is to assume that the fourth-order

crack density tensor $\beta = 0$ (Sayers and Kachanov 1995) this follows from the fact that β enters the elastic potential (or elastic compliances) with a relatively small multiplier. For an isotropic distribution of microcrack orientations, this implies that the ratio of Young's modulus to Poisson's ratio is independent of damage, i.e.,

$$\frac{\nu}{E} = \frac{\tilde{\nu}}{\tilde{E}},$$

which contrasts with the assumption made in the CDM approach where $\nu = \tilde{\nu}$. In the micromechanical approach, the assumption $\beta = 0$ also implies that the second-order crack density tensor α_{ij} remains the sole crack variable, and for an isotropic cracked material, this tensor reduces to a single scalar crack density variable α^{SC}.

Using the known values of K_{exp} and G_{exp} for the defect-less fused aggregate of pure calcite grains, and $\tilde{K}_{\text{exp}}$ and $\tilde{G}_{\text{exp}}$ calculated from the ultrasonic and density data reported by Sarout et al. (2017) on the CM specimen under increasing confining pressure, and using Eq. (11) allows us to estimate α^{SC} independently from the bulk modulus data on one hand, and from the shear modulus data on the other, i.e.,

$$\begin{aligned} \alpha_K^{SC} &\approx \frac{1}{3}\left(\frac{1}{\tilde{K}_{\text{exp}}} - \frac{1}{K_{\text{exp}}}\right), \\ \alpha_G^{SC} &\approx \frac{1}{2}\left(\frac{1}{\tilde{G}_{\text{exp}}} - \frac{1}{G_{\text{exp}}}\right). \end{aligned} \tag{13}$$

Let us again consider two approaches for estimating the scalar damage variable from laboratory data. The first method makes use of both P- and S-wave velocity input data to compute the independent bulk and shear of the isotropic rock in the intact and damaged states. Equation (13) is then used to calculate the corresponding α_K^{SC} and α_G^{SC}. Finally, the experimentally-determined scalar damage variable is taken as the average of α_K^{SC} and α_G^{SC}, i.e.,

$$\begin{aligned} \alpha^{SC} &\approx \frac{1}{2}\left(\alpha_K^{SC} + \alpha_G^{SC}\right), \\ &\approx \frac{1}{6}\left(\frac{1}{\tilde{K}_{\text{exp}}} - \frac{1}{K_{\text{exp}}}\right) + \frac{1}{4}\left(\frac{1}{\tilde{G}_{\text{exp}}} - \frac{1}{G_{\text{exp}}}\right). \end{aligned} \tag{14}$$

In order to better compare our results with previous data and models (e.g., Mondal et al. 2019, 2020) we also consider a second approximate crack density variable $\alpha_{E\,\text{exp}}^{SC}$ directly based on experimentally-determined Young's modulus (intact and damaged states). Using Eq. (11) to compute Young's modulus with $\beta = 0$ yields

$$\begin{aligned} \alpha_E^{SC} &\approx \frac{1}{\tilde{E}_{\text{exp}}} - \frac{1}{E_{\text{exp}}}, \\ &\approx \frac{1}{9}\left(\frac{1}{\tilde{K}_{\text{exp}}} - \frac{1}{K_{\text{exp}}}\right) + \frac{1}{3}\left(\frac{1}{\tilde{G}_{\text{exp}}} - \frac{1}{G_{\text{exp}}}\right). \end{aligned} \tag{15}$$

which contrasts with the definition of D_E^{SC} in Eq. (8) for the CDM approach, and shows that these two approximate scalar variables are related through

$$D_E^{SC} = \tilde{E}\,\alpha_E^{SC}, \tag{16}$$

where the damage variable D_E^{SC} is dimensionless, and the crack density variable bears the units of a compliance (Pa^{-1}).

Note that K_{exp} and G_{exp} are the elastic moduli of the intact (undamaged) rock material; and $\tilde{K}_{\text{exp}}$ and $\tilde{G}_{\text{exp}}$ are the elastic moduli of the damaged rock material estimated from laboratory ultrasonic and density data under increasing confining pressure by Sarout et al. (2017). Because Carrara marble is made of 98% calcite, the intact material properties are derived form the properties of a fused aggregate of randomly-oriented calcite grains with no porosity, no microcracks or other defects ($K_{\text{calcite}} = 80\,\text{GPa}$, and $G_{\text{calcite}} = 30\,\text{GPa}$).

4 Results: Impact of Thermal Damage and Microcrack Closure with Increasing Pressure

The thermally cracked CM sample is subjected to a stepwise increase in confining pressure, and at each pressure increment the ultrasonic P- and S-wave velocities are measured using the pulse-transmission technique (Birch 1960). Two ultrasonic transducers (0.5 MHz central resonant frequency) are located at the top and bottom end of the cylindrical rock sample, respectively. One transducer acts as a source and transmits a mechanical vibration (longitudinal P or shear S); and the other transducer acts as a receiver of the P- or S- vibration transmitted through the length of the sample. Dual P and S Panametrics ultrasonic transducers were used, with a resonant frequency centred around 0.5MHz. They were embedded in the top and bottom steel platens within the pressure vessel (see Fig. 2 in Sarout et al. (2017)). These dual transducers are made of two separate/independent piezoceramics with contrasting normal (P) and shear (S) polarization. The dominant frequency of the source voltage supplied to the piezoceramics is also 0.5MHz, and the 500 Volts pulse is a negative square function. The P and S piezoceramics are excited separately/independently/consecutively. For each ultrasonic transmission mode (P-to-P or S-to-S), multiple shots were generated by the source transducer, and the transmitted pulses were recorded by the corresponding

receiver and stacked/averaged to improve the signal to noise ratio of the recorded waveform. The flight-time of the P phase is determined form the recorded P waveform, and that of the S phase from the independently-recorded S waveform. Knowledge of the transmission time for each wave phase (P or S) on the recorded waveform, and the propagation distance (sample length) allows for the calculation of the sought P- and S-wave velocities. The elastic moduli are estimated from these velocities and the density of the rock.

All the elastic parameters of this isotropic and thermally cracked CM specimen can be calculated for any level of confining pressure from the P-wave velocity V_P, S-wave velocity V_S, and the known density ρ of the specimen, accounting for the increase in density with increasing confining pressure and strain hardening (Sarout et al. 2017). Once the velocity of the longitudinal ultrasonic wave (P-wave) and that of the shear ultrasonic wave (S-wave) are measured (together with the density of the rock), the coefficients of the elastic stiffness tensor and hence the elastic moduli can be calculated from the well-known Christoffel's equations for elastic wave propagation in isotropic elastic solids (e.g., Eslami et al. 2010):

$$\tilde{K} = \rho\left(V_P^2 - \frac{4}{3}V_S^2\right),$$
$$\tilde{G} = \rho V_S^2.$$

where the two independent elastic moduli $\tilde{K}$ and $\tilde{G}$ are readily calculated from the two independent ultrasonic wave velocities V_P and V_S and the density measured in the laboratory for the isotropic and thermally cracked CM specimen subjected to increasing confining pressure.

Using these laboratory ultrasonic and density data, we invert the damage and crack density variables for the complete tensorial models and for their respective scalar approximations. Figure 2 summarises these results and shows the evolution of D_1, D_2, D^{SC}, D_E^{SC}, α, β, α^{SC}, α_E^{SC} as a function of confining pressure. With increasing confining pressure the absolute value of all laboratory-derived damage/crack density parameters decreases asymptotically towards a low or zero value. Most of the decrease, more than 75%, is recorded in the interval 0 to 15 MPa. All the damage parameters but D_2 for the complete tensorial model, and for its scalar approximations in the CDM approach tend toward a non-zero asymptotic value at high confining pressure. In contrast, all the crack density parameters for the complete tensorial model, and for its scalar approximations in the EMT approach cancel at high pressure (tend toward a zero asymptote).

Using these inverted values of damage and crack density variables, we can compute the corresponding predictions of the complete tensorial and approximate scalar models for both the CDM and EMT approaches. Figure 3 summarises these results and compares the predictions of all models in terms of bulk, shear, Young's and P-wave moduli, as well as in terms of Poisson's ratio. The uncertainty (error bars) of the laboratory-derived elastic moduli in Fig. 3 are calculated using the approximate formula for propagation of errors for a multivariable function from Hughes and Hase (2010) (equation 4.16). We observe that both tensorial models, involving two damage or crack density parameters, fit equally well and perfectly the laboratory data of the cracked CM specimen at all confining pressures. For the predictions of shear and Young's moduli G and E, all approximate scalar models perform similarly well. However, for the bulk modulus, the P-wave modulus and Poisson's ratio, the scalar approximations derived from the CDM approach in terms of D^{SC} or D_E^{SC} perform significantly better than the corresponding scalar approximations derived from the EMT method in terms of α^{SC} or α_E^{SC}. This laboratory dataset and the modelling and inversion results presented here suggest that the assumption of a constant Poisson's ratio (independent of damage) in the CDM approach leads to a more accurate approximation of the actual moduli of the cracked CM specimen with a single scalar parameter D^{SC} or D_E^{SC}, than the corresponding scalar approximation derived from the EMT approach with a single scalar crack density α^{SC} or α_E^{SC}.

In addition, Fig. 4 shows the regression line between the tensorial damage variable D_1 and the two scalar damage variables D^{SC} and D_E^{SC} with the 95% prediction interval. From this figure and the Pearson correlation coefficients ($R = 0.9968$ for D^{SC} and $R = 0.9987$ for D_E^{SC}), the slopes (1.06 and 0.96 respectively) and y-intercepts ($-$ 0.02e and 0.01 respectively) we can conclude that the scalar damage variable calculated using either approximation give a very close fit.

5 Discussion

5.1 Validity of Scalar Model Assumptions

Figure 5 shows that for a confining pressure higher than about 5 MPa the values derived from laboratory data on the CM specimen for ν and above 10 MPa for ν/E values are nearly constant. In this pressure range, the assumptions of both approaches seem reasonable in view of the ultrasonic and density data available; only at pressures below 5 to 10 MPa ν and ν/E depart measurably from a constant value. Figure 5 shows the limitations of the assumptions underlying the single-scalar approximation version of the CDM (ν constant) and EMT (E/ν constant) models. It shows that the assumption for each approximate model is valid in practice only above 5 to 10 MPa of applied confining pressure. These observations are based on actual laboratory measurements conducted on the cracked rock under variable confining

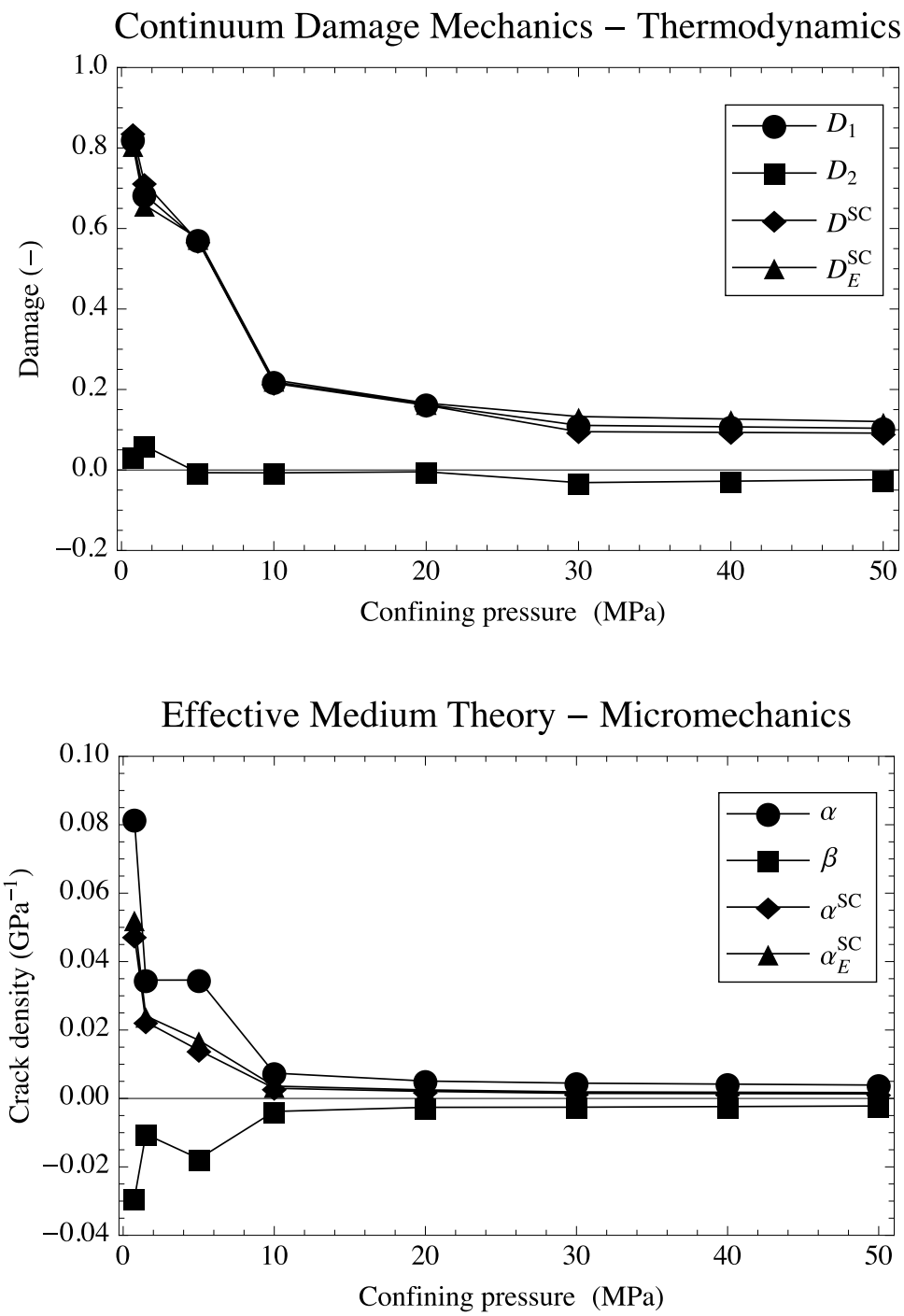

Fig. 2 Comparison of the damage and crack density parameters inverted from laboratory ultrasonic and density data on an isotropic and thermally cracked Carrara marble specimen (Sarout et al. 2017) using: (i) tensorial models (with D_1 and D_2 or α and β); or (ii) approximate scalar models with either D^{SC} or D_E^{SC} as damage variables; or with either α^{SC} or α_E^{SC} as crack density variables

pressure. At these low pressures it is recommended to use the complete tensorial damage or crack density models rather than their single-scalar approximation.

5.2 Irreversible Thermal Damage and Reversible Microcrack Closure

Let us consider the two extreme situations reported in this laboratory dataset at the highest (50 MPa) and lowest (0.7 MPa) confining pressure values. Table 1 displays the values of the damage variables D_1 and D_2 for the thermally cracked CM specimen at the lowest confining pressure available (0.7MPa), where the microcracks are open. Similarly, Table 2 displays the values of these damage parameters at the highest confining pressure available (50 MPa). We observe that for the most part the scalar damage values are reasonably close to the tensorial damage values. The moduli of the intact aggregate of fused calcite grains without defects

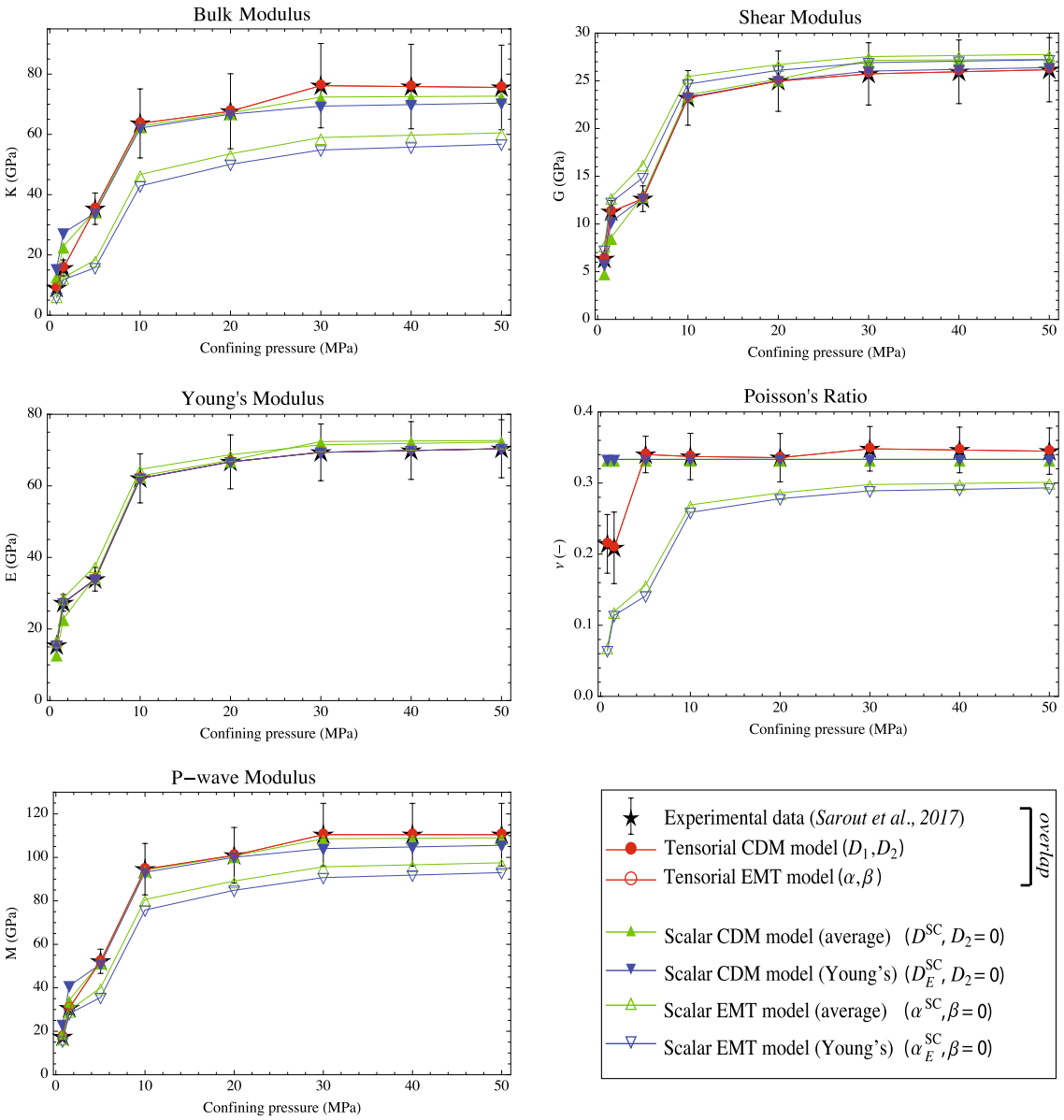

Fig. 3 Comparison of laboratory-derived and predicted elastic moduli of the thermally cracked Carrara marble specimen (Sarout et al. 2017)

are also reported in these tables ($K_{\text{calcite}} = 80\,\text{GPa}$, and $G_{\text{calcite}} = 30\,\text{GPa}$). At the highest confining pressure of 50 MPa, we observe that all the elastic moduli calculated using the scalar damage models are within 7% of the tensorial values. At the lowest confining pressure of 0.7 MPa, significant discrepancy arises between the tensorial damage values and their approximate scalar values, especially for Poisson's ratio ν, the bulk modulus K and Lamé parameter λ. In these tables and in Fig. 3 we report the error bars using the approximate formula for propagation of errors for a multivariable function from Hughes and Hase (2010) (Eq. 4.16). This formula has some limitations and assumes that the magnitude of the error is small.

The results reported so far suggest that with confining pressure increase the elastic moduli tend toward an asymptotic value close to that expected for a defect-less aggregate of fused calcite grains, but not quite the same. Therefore, we can confidently assume that the effect of microcrack closure can be neglected once the confining pressure has increased above about 15 to 20 MPa (see Fig. 3), which reflects progressive crack closure under increasing confining pressure. For high confining pressures above this threshold we observe that: (i) Poisson's ratio reaches the constant value of the defect-less rock; (ii) an asymptotic difference in elastic moduli with the defect-less rock remains and is attributed

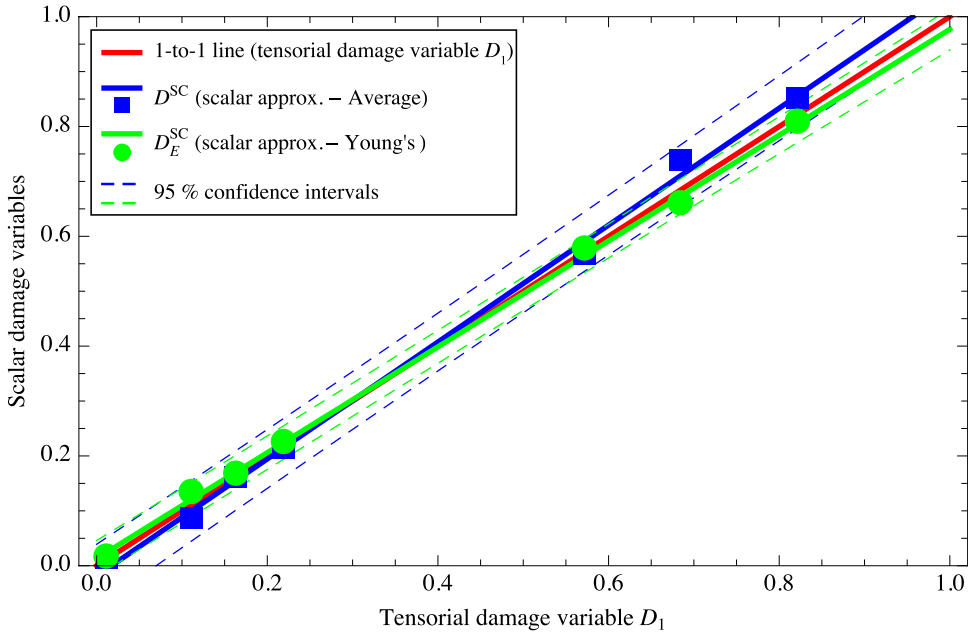

Fig. 4 Linear fit (with 95% prediction interval) of the scalar damage variables (D^{SC}, D_E^{SC}) with the tensorial damage variable D_1 for the thermally cracked dry Carrara marble specimen under increasing confining pressure

to the irreversible damage induced by thermal cracking. Table 2 reports the change in the elastic moduli at the highest confining pressure recorded where we assume that the microcracks have closed at least partially since the elastic moduli reach a stable asymptotic value. It also shows that the elastic moduli most reduced by the irreversible damage was the Young's modulus (by 12%) whereas the elastic moduli least affected by the irreversible damage was Poisson's ratio which remained almost constant. In contrast at low confining pressures where we can assume that a number of microcracks are still open we assume that the ultrasonic measurements record the cumulative effect of reversible microcrack closure and irreversible damage (non-recoverable by pressure increase).

Using a scalar variable to describe damage and microcrack closure in the CDM approach assumes that all the elastic moduli are increased in the same proportion, except Poisson's ratio, which remains constant by assumption. In contrast, when a tensor is used to describe microcrack closure (and both D_1 and D_2 or α and β are non-zero) all the elastic moduli are affected by damage to varying degrees. In other words, once confining pressure has increased above about 15 MPa, so that the elastic moduli plateau and remain constant, we can isolate the effect of irreversible damage due to thermal cracking, i.e., the observed asymptotic difference with the elastic moduli of the defect-less rock.

6 Conclusion

Overall, this laboratory dataset and the CDM and EMT modelling and inversion results presented here suggest that: (i) irreversible thermal cracking and microcrack opening occur after heating and sudden cooling of the CM specimen, whereas reversible and progressive microcracks' closure occurs with increasing pressure; (ii) both tensorial damage/cracking models involving two damage/crack density variables fit equally well (perfectly as expected for isotropic damage) the laboratory data at any confining pressure; (iii) single scalar approximation models can be accurate for damage predictions compared to their complete tensorial counterparts, which is particularly true for the CDM approach; (iv) single scalar approximations derived from the CDM approach, and assuming a constant Poisson's ratio of the cracked rock, better predicts all elastic moduli than the corresponding scalar approximation derived from the EMT approach, where a constant ratio of Young's modulus to Poisson's ratio is assumed instead; and (v) it is more reliable to use a tensorial rather than a scalar description of the effect of reversible microcrack closure with pressure on all elastic parameters, including Poisson's ratio. If the impact of reversible microcrack closure is accounted for, then a single scalar description of irreversible thermal damage is remarkably accurate.

This work highlights the need to account for reversible crack closure and opening in models of damage and healing in naturally fractured rocks or engineered composites

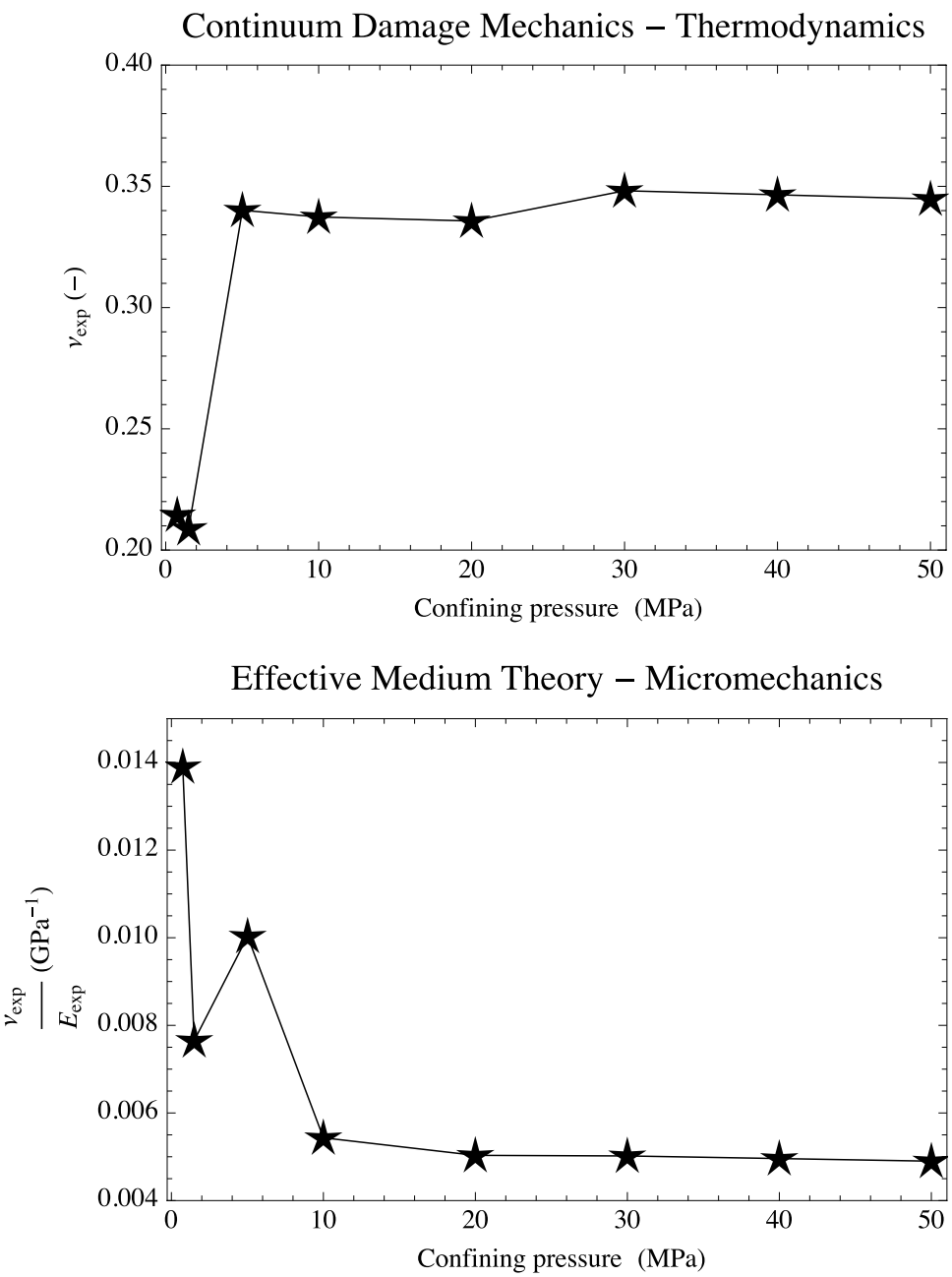

Fig. 5 Evolution of Poisson's ratio ν and the ratio of Young's modulus to Poisson's ratio E/ν derived from experimental data. Note that the scalar approximation of the continuum damage model assumes that Poisson's ratio is constant $\nu = \tilde{\nu}$ (independent of damage); the scalar approximation of the effective medium model assumes that the ratio of Young's modulus to Poisson's ratio $\nu/E = \tilde{\nu}/\tilde{E}$ (independent of crack density)

Table 1 Comparison of tensorial and scalar damage models in the CDM approach at low confining pressure (0.7MPa)

Parameter	Intact CM	Tensorial model	Scalar model (average)	Scalar model (Young's)
λ (GPa)	60	4.8 ± 1.4	9.0 ± 0.6	11.6 ± 0.2
G (GPa)	30	6.4 ± 0.6	4.5 ± 0.3	5.8 ± 0.1
E (GPa)	80	15.4 ± 1.2	11.9 ± 0.8	15.4 ± 0.3
K (GPa)	80	9.0 ± 1.4	11.9 ± 0.8	15.4 ± 0.3
ν	0.33	0.21 ± 0.04	0.33	0.33
D_1	0	0.82 ± 0.02	0.85 ± 0.01	0.81 ± 0.02
D_2	0	0.03 ± 0.008	0	0

Table 2 Comparison of tensorial and scalar damage models in the CDM approach at high confining pressure (50MPa)

Parameter	Intact values	Tensorial damage	Scalar damage (average)	Scalar damage (Young's)
λ (GPa)	60	58.1 ± 14.4	55.0 ± 5.0	52.8 ± 1.5
G (GPa)	30	26.2 ± 3.4	27.5 ± 2.5	26.4 ± 0.8
E (GPa)	80	70.4 ± 8.1	73.3 ± 6.7	70.4 ± 2.0
K (GPa)	80	75.6 ± 14.0	73.3 ± 6.7	70.4 ± 2.0
ν	0.33	0.34 ± 0.03	0.33	0.33
D_1	0	0.10 ± 0.10	0.08 ± 0.08 0.08	0.12 ± 0.10
D_2	0	-0.02 ± 0.07	0	0

when using ultrasonic measurements to develop phenomenological models. Accounting for, and discriminating between these two processes is not only important for modelling and prediction purposes, but also for analyzing ultrasonic data, which can only record their cumulative effects.

Acknowledgements This research is supported by the Australian Research Council Discovery Early Career Researcher Award DE140404398. We acknowledge the financial support provided by CSIRO's Onshore Gas Program through a Strategic Research Fund, and the assistance of the technical officers of CSIRO's Geomechanics and Geophysics Laboratory: Bruce Maney, Shane Kager, Leigh Kiewiet, Stephen Firns, and David Nguyen.

Declarations

Conflict of interest The authors declare that they have no conflict of interest.

References

Ahn E, Kim H, Sim SH, Shin S, Shin M (2017) Principles and applications of ultrasonic-based nondestructive methods for self-healing in cementitious materials. Materials 10:278. https://doi.org/10.3390/ma10030278

Audoin B, Baste S (1994) Ultrasonic evaluation of stiffness tensor changes and associated anisotropic damage in a ceramic matrix composite. J Appl Mech 61:309

Birch F (1960) The velocity of compressional waves in rocks to 10 kilobars: 1. J Geophys Res 65:1083

Brantut N (2015) Time-dependent recovery of microcrack damage and seismic wave speeds in deformed limestone. J Geophys Res pp 8088–8109, https://doi.org/10.1002/2015JB012324

Bristow J (1960) Microcracks, and the static and dynamic elastic constants of annealed and heavily cold-worked metals. Br J Appl Phys 11:81

Case E (1984) The effect of microcracking upon the Poissons ratio for brittle materials. J Mater Sci 19:3702

Castellano A, Fraddosio A, Piccioni M (2017) Ultrasonic goniometric immersion tests for the characterization of fatigue post-lvi damage induced anisotropy superimposed to the constitutive anisotropy of polymer composites. Compos B 116:122

Cauvin A, Testa R (1999a) Damage mechanics basic variables in continuum theories. Int J Solids Struct 36:747–761

Cauvin A, Testa R (1999b) Elastoplastic material with isotropic damage. Int J Solids Struct 36:727–746

Curie P (1894) Sur la symétrie dans les phénomènes physiques, symétrie dun champ électrique et dun champ magnétique. Journal de Physique Théorique et Appliquée 3:393–415

Eshelby JD (1957) The determination of the elastic field of an ellipsoidal inclusion, and related problems. Proc R Soc London Ser A 241(1226):376. https://doi.org/10.1098/rspa.1957.0133

Eslami J, Grgic D, Hoxha D (2010) Estimation of the damage of a porous limestone from continuous (p- and s-) wave velocity measurements under uniaxial loading and different hydrous conditions. Geophys J Int 183:1362–1375. https://doi.org/10.1111/j.1365-246X.2010.04801.x

Grechka V, Kachanov M (2006) Effective elasticity of rocks with closely spaced and intersecting cracks. Geophysics 71:D85–D91

Helbig K (1994) Foundations of anisotropy for exploration seismics. Pergamon

Hufenbach W, Böhm R, Langkamp A, Kroll L, Ritsche T (2006) Ultrasonic evaluation of anisotropic damage in multiaxially textile reinforced themoplastic hybrid composites made by hybrid yarns. Mech Compos Mat 42:151

Hughes I, Hase T (2010) Measurements and their uncertainties A Practical Guide to Modern Error Analysis. Oxford

Kachanov M (1980) Continuum model of medium with cracks. J Eng Mech Div 106:1039–1051

Kachanov M (1993) Elastic solids with many cracks and related problems. Adv Appl Mech 30:259–445

Kaproth B, Marone C (2014) Evolution of elastic wave speed during shear-induced damage and healing within laboratory fault zones. J Geophys Res: Solid Earth pp 4821–4840, https://doi.org/10.1002/2014JB011051

Lemaitre J (1996) A course on damage mechanics. Springer-Verlag, New York

Li LC, Tang CA, Li G, Wang SY, Liang ZZ, Zhang YB (2012) Numerical simulation of 3d hydraulic fracturing based on an improved flow-stress-damage model and a parallel fem technique. Rock Mech Rock Eng 45(5):801–818

Mondal S, Olsen-Kettle L, Gross L (2019) Simulating damage evolution and fracture propagation in sandstone containing a preexisting 3-d surface flaw under uniaxial compression. Int J Numer Anal Meth Geomech 43(7):1448–1466

Mondal S, Olsen-Kettle L, Gross L (2020) Regularization of continuum damage mechanics models for 3-d brittle materials using implicit gradient enhancement. Comput Geotech 122:103505

Murakami S (2012) Continuum damage mechanics A Continuum Mechanics Approach to the Analysis of Damage and Fracture. Springer, New York

Olsen-Kettle L (2018a) Bridging the macro to mesoscale: Evaluating the fourth order anisotropic damage tensor parameters from ultrasound measurements of an isotropic solid under triaxial

stress loading. Int J Damage Mech. https://doi.org/10.1177/1056789518757293
Olsen-Kettle L (2018b) Quantifying the orthotropic damage tensor for composites undergoing damage-induced anisotropy using ultrasonic investigations, manuscript submitted for publication
Olsen-Kettle L (2018c) Using ultrasonic investigations to develop anisotropic damage models for initially transverse isotropic materials undergoing damage to remain transverse isotropic. I J Solids Struct 138:155–165. https://doi.org/10.1016/j.ijsolstr.2018.01.007
Ouarabi M, Antonaci P, Boubenider F, Gliozzi A, Scalerandi M (2017) Ultrasonic monitoring of the interaction between cement matrix and alkaline silicate solution in self-healing systems. Materials 10:46. https://doi.org/10.3390/ma10010046
Rasolofosaon P (1998) Stress-induced seismic anisotropy revisited. Revue De LInstitut Francais du Pétrole 53:679–692
Sarout J, Molez L, Guéguen HN (2007) Shale dynamic properties and anisotropy under triaxial loading: experimental and theoretical investigations. Phys Chem Earth 32:896–906. https://doi.org/10.1016/j.pce.2006.01.007
Sarout J, Cazes E, Piane CD, Arena A, Esteban L (2017) Stress-dependent permeability and wave dispersion in tight cracked rocks: Experimental validation of simple effective medium models. J Geophys Res. https://doi.org/10.1002/2017JB014147
Sayers C, Kachanov M (1995) Microcrack-induced elastic wave anisotropy of brittle rocks. J Geophys Res 100(B3):4149–4156
Voigt W (1910) Lehrbuch der kristallphysik. Teubner, Leipzig
Walsh J (1965a) The effect of cracks in rocks on Poissons ratio. J Geophys Res 70:5249
Walsh J (1965b) The effect of cracks on the compressibility of rock. J Geophys Res 70:381
Zhu W, Tang C (2004) Micromechanical model for simulating the fracture process of rock. Rock Mech Rock Eng 37:25–56. https://doi.org/10.1007/s00603-003-0014-z
Zimmerman R (1985) The effect of microcracks on the elastic moduli of brittle materials. J Mater Sci Lett 4:1457